Ni-Cu and Ni-Co-Modified Fly Ash Zeolite Catalysts for Selective Hydrodeoxygenation of Levulinic Acid to γ-Valerolactone

Margarita Popova *, Momtchil Dimitrov, Silviya Boycheva, Ivan Dimitrov, Filip Ublekov, Neli Koseva, Genoveva Atanasova, Ágnes Szegedi *

Posted Date: 1 December 2023

doi: 10.20944/preprints202312.0001.v1

Keywords: lignocellulosic biomass; levulinic acid; fly ash zeolite; γ-valerolactone; Co-Ni alloy

Article

Ni-Cu and Ni-Co-Modified Fly Ash Zeolite Catalysts for Selective Hydrodeoxygenation of Levulinic Acid to γ-Valerolactone

Margarita Popova [1,*], Momtchil Dimitrov [1], Silviya Boycheva [2], Ivan Dimitrov [1], Filip Ublekov [3], Neli Koseva [3], Genoveva Atanasova [4] and Ágnes Szegedi [5,*]

[1] Institute of Organic Chemistry with Centre of Phytochemistry, Bulgarian Academy of Sciences, 1113 Sofia, Bulgaria;
[2] Technical University, Sofia
[3] Institute of Polymers, Bulgarian Academy of Sciences, Sofia
[4] Institute of General and Inorganic Chemistry, Bulgarian Academy of Sciences, Sofia
[5] HUN-REN, Research Centre for Natural Sciences, Institute of Materials and Environmental Chemistry, Magyar tudósok krt. 2., 1117 Budapest, Hungary
* Correspondence: margarita.popova@orgchm.bas.bg (M.P.); szegedi.agnes@ttk.hu (A.S.)

Abstract: Monometallic (Ni, Co, Cu) and bimetallic (Ni-Co, Ni-Cu) 10-20 wt. % metal containing catalysts supported on fly ash zeolite were prepared by post-synthesis impregnation method. The catalysts were characterized by X-ray powder diffraction, N_2 physisorption, XPS and H_2-TPR methods. Finely dispersed metal oxides and mixed oxides were detected after the decomposition of impregnating salt on the relevant zeolite support. By reduction intermetallic, NiCo and NiCu phases were identified in the bimetallic catalysts. Hydrogeoxygenation of lignocellulosic biomass-derived levulinic acid to γ-valerolactone (GVL) was studied. Bimetallic, 10 wt. % Ni, 10 wt. % Cu or Co containing fly ash zeolite catalyst showed higher catalytic activity than monometallic ones. Their selectivity to GVL reached 70–85% at 100% conversion. The reaction proceeds through formation of 4-hydroxy pentanoic acid, as the only intermediate compound.

Keywords: lignocellulosic biomass; levulinic acid; fly ash zeolite; γ-valerolactone; Co-Ni alloy

1. Introduction

Lignocellulosic biomass is a promising alternative to fossil fuel sources because of the increased demand of energy and declining supplies [1–3]. Another essential aspect in energy production is the prevention of greenhouse gas emissions, as the biomass and biomass-derived fuels are considered carbon neutral. Direct combustion of biomass, however, is not energy efficient, due to its high moisture content and low volumetric energy density, therefore the possibility of its conversion into liquid or gaseous fuels, so called biofuels, are being intensively investigated [4,5]. Catalysis plays a crucial role in processing biomass into fuels, their precursors or platform molecules [6,7]. An important step of biomass valorization is the hydrolysis of lignocellulose into a mixture of cellulose, hemicellulose and lignin, and further transformations to C5 and C6 monosaccharides [8]. Among platform molecules, which are produced from biomass, levulinic acid (LVA) is one of the most important for production of valuable products, such as biofuels, solvents, intermediate for pharmacy etc. [9–12]. LVA is considered as a chemical building block because it contains keto and carboxyl groups in its structure, which enables its conversion into a wide range of derivatives. Moreover, it is one of the top value-added sustainable chemical compounds that is produced from abundant renewable resources [13]. Hydrodeoxygenation of LVA to γ-valerolactone (GVL) is an important process because it can be used as a solvent, fuel additive, or intermediate in the production of diverse value-added chemicals. The hydrodeoxygenation of LVA to GVL has been performed in gaseous or in liquid media by applying homogeneous or heterogeneous catalysts [14]. Another issue is the energy efficiency of hydrogen supply for the hydrodeoxygenation process through alcohols, formic acid or molecular hydrogen [15–17]. Hydrogen can also be produced by catalytic steam reforming of

 doi:10.20944/preprints202312.0001.v1

biomass derived LVA, which allows the integration of the hydrogen production with the hydrogenation processes [18].

The synthesis of heterogeneous catalysts is prioritized as alternative to the more expensive and unrecoverable homogeneous ones used in continuous flow organic transformations. Heterogeneous catalytic processes offer advantages such as easy recovery and recycling. Among them the supported noble metal (Ru, Ir, and Pd), or transition metal ones such as Co, Cu, and Ni show the best catalytic results [12,19–21]. Although noble metals show excellent activity and selectivity in the hydrodeoxygenation of LVA to GVL, the industrial use of these catalysts is expensive, and to improve the economic efficiency of the process, it is more expedient to replace them with more cost-effective ones [22]. Another drawback is the metal leaching in severe reaction conditions, which together with their high price limit the applications of noble metals in industrial scales. The development of active and cheap catalyst for the preparation of GVL by hydrodeoxygenation of LVA requires the optimization of reaction parameters, and the type of metals and catalyst carrier [23]. Several studies evidence the efficiency of transition metals and their oxides in the catalytic hydrodeoxygenation of LVA to GVL. Almost complete LVA selective conversion has been reported for Ni catalysts supported on various carriers and heterostructured Ni/NiO composites [24,25]. Superior performance of bimetallic transition metal catalysts has been also observed compared to monometallic ones, for example iron-based bimetallic species supported on ceramics reaching over 95% conversion of LVA to GVL at 180 °C and 40 bar H_2 pressure, because of the strong synergy of iron oxides with other metal catalysts [26]. Bimetallic Ni-Cu/Al_2O_3 and Ni-Co/Al_2O_3 have shown 100% conversion rate at very high selectivity for GVL formation [27]. Vapor-phase hydrodeoxygenation of LVA to GVL has been performed over bimetallic Cu-Co/Al_2O_3, with selectivity higher than 99% at 250 °C [28]. The surface morphology, ratio, and electronic structure of Brønsted/Lewis acid pairs and Lewis acid/base pairs has been observed as a crucible for the total LVA to GVL conversion process, including hydrogen generation, transfer, and the hydrogenation with transition metal catalysts [29]. The modification of zeolites with noble or transition metals is a promising way for preparation of catalyst requiring metallic and acidic functionalities [30]. Faujasite-type zeolites (X or Y) are one of the most studied catalytic supports, due to the possibilities of controlling their catalytic efficiency and selectivity by modification with metal oxides, due to their supercell structure that can host large diameter molecules and particles, by ion exchange with metal cations or by controlling the Si/Al ratio in the synthesis to achieve appropriate acidity [31]. Metal ions and metal particles in extra-framework positions also have favorable effect on the catalytic behavior [32]. Finally, environmental safety of zeolites is important factor, even if they are obtained from waste aluminosilicates [33]. The ecological impact of biofuels will be even more significant if we use catalysts that are based on economically profitable and abundantly available waste sources. The approach to obtain efficient and cost-effective catalysts for LVA hydrodeoxygenation to GVL by utilizing solid-phase wastes such as waste incineration fly ash, sewage sludge, and contaminated soil has been reported [34]. The published results reveal 94% conversion efficiency for zeolite-like frameworks with insufficient surface characteristics modified with NiO [34]. Sulfonic acid functionalized polystyrene coated coal fly ash catalyst have been developed for esterification of LVA with n-butanol to alkyl levulinates fuel with 99.6% conversion rate at mild conditions [35]. Solid acid composite catalyst developed on the basis of coal fly ash have shown promising results as catalysts in biomass conversion processes [36]. Unprocessed coal fly ash, however, is characterized by large non-uniformity in its morphology, structure and composition, and reproducibility can hardly be achieved [37]. In our previous studies, high catalytic activity was found on zeolites obtained from coal fly ash in the oxidation of volatile organic compounds [38]. Coal fly ash zeolites (CFAZ) are self-organized catalytic systems that contain a zeolite phase as a catalytic support with active centers of finely dispersed iron oxide species and framework/extra-framework iron ions incorporated in the zeolite lattice [39]. CFAZ can be easily modified to bimetallic catalysts by post-synthesis impregnation with metal salts and their subsequent reduction to metal oxides, thus increasing their catalytic activity [32]. The processing of coal fly ash into zeolites by double stage alkaline synthesis with ultrasonic homogenization of the reaction mixtures provides several product advantages compared to the raw coal ash, such as: tens of times

 doi:10.20944/preprints202312.0001.v1

higher specific surface area, mixed micro-mesoporous structure, homogeneous distribution of iron oxide phases, high thermal stability and chemical inertness, reduced leaching of metal particles, etc. [40–42]. The favorable surface characteristics of zeolite-like materials in combination with the uniformly incorporated catalytic sites of iron ions and oxide nanoparticles can be useful tools to develop cheap and efficient catalysts. The self-organized catalytic system can be easily modified in order to get bimetallic, highly active catalytic centers for the improvement of catalytic performance.

In the present study, monometallic and bimetallic Ni, Cu and Co functionalized fly ash zeolites were prepared by post synthesis impregnation and were studied in hydrodeoxygenation of levulinic acid to γ-valerolactone.

2. Experimental part

2.1. Materials

The raw material for the preparation of the catalysts is coal fly ash collected from the electrostatic precipitators of one of the large combustion plants in Bulgaria TPP "AES Galabovo", burning lignite coal. CFA has been studied in depth in our previous publications with respect to chemical and phase composition and morphology [43,44]. It is a high silica CFA grade F, according to ASTM C618 standard, containing about 74 wt. % SiO_2+Al_2O_3, of which 50 wt. % is SiO_2. CFA has a low CaO content of up to 4.5 wt. % and includes a larger amount of iron oxide phases, expressed as Fe_2O_3, approx. 13 wt. %. As a result of the specifics of the steam generator, CFA is highly amorphized, but can contain some crystalline phases such as quartz, mullite, magnetite and portlandite [44,45].

2.2. Synthesis of coal fly ash zeolite

The initial zeolite from coal ash, denoted **Z**, was synthesized by ultrasound-assisted two-step synthesis comprising of hydrothermal activation with pre-alkaline fusion. Coal fly ash and sodium hydroxide used as an alkaline activator were mixed in an appropriate ratio and calcined at 550 °C for 1 h. The cooled batch is crushed, mixed with distilled water to a medium alkalinity of 2.3 mol/l and homogenized by ultrasonic treatment for 15 min. The resulting suspension is aged for 8 h and subjected to hydrothermal activation at 90 °C for 4 h. The obtained powdery product is removed by filtration, washed with distilled water until neutral, dried at 105 °C and proceeded for further studies. This well-established and optimized laboratory procedure for coal fly ash alkaline conversion yields high-quality zeolite X as a single crystalline phase with surface characteristics favorable for catalytic applications [40,43].

2.3. Impregnation of coal fly ash zeolite with Ni, Co and Cu

An impregnation technique with nickel, cobalt and copper salts was applied for loading of 10 wt. % metals, respectively. The zeolite support was dehydrated at 160 °C for 2 h before the impregnation procedure.

2.3.1. Preparation of monometallic fly ash zeolite catalysts

A 10 wt. % Ni containing fly ash zeolite was prepared by the following procedure: 550 mg $Ni(NO_3)_2 \cdot 6\,H_2O$ was dissolved in 5 mL ethanol and was added to 1 g zeolite support by stirring until evaporation of the solvent. Then the sample was dried at 80 °C for 18 h and calcined at 450 °C for 3 h with a rate of 1 °C/min. The sample was denoted as **10Ni/Z**.

A 10 wt.% Co-modified fly ash zeolite was prepared by the following procedure: 548.2 mg $Co(NO_3)_2 \cdot 6\,H_2O$ was dissolved in 5 mL ethanol and was added to 1 g AES0 support by stirring until evaporation of the solvent. Then the sample was dried at 80 °C for 18 h and calcined at 450 °C for 3 h with a rate of 1 °C/min. The sample was denoted as **10Co/Z**.

A 10 wt. % Cu-modified fly ash zeolite was prepared by the following procedure: 516.4 mg $Cu(NO_3)_2 \cdot 6\,H_2O$ was dissolved in 5 mL ethanol and was added to 1 g zeolite support by stirring until

 doi:10.20944/preprints202312.0001.v1

evaporation of the solvent. Then the sample was dried at 80 °C for 18 h and calcined at 450 °C for 3 h with a rate of 1 °C/min. The sample was denoted as **10Cu/Z**.

2.3.2. Preparation of bimetallic fly ash zeolite catalysts

Bimetallic, 5 or 10 wt. % Ni- and Co-modified fly ash zeolite was prepared by the following procedure: 275/550 mg $Ni(NO_3)_2 \cdot 6\,H_2O$ and 274.1/548.2 mg $Co(NO_3)_2 \cdot 6\,H_2O$ dissolved in 5 mL ethanol was added to 1 g fly ash zeolite sample and then was dried at 80 °C for 18 h. The precursor salts were decomposed in air at 450 °C with a rate of 1 °C/min for 3h. The samples were denoted as **5Ni5Co/Z** and **10Ni10Co/Z**, respectively.

Bimetallic, 5 or 10 wt. % Ni- and Cu-modified fly ash zeolite was prepared by the following procedure: 275/550 mg $Ni(NO_3)_2 \cdot 6\,H_2O$ and 258.2/516 mg $Cu(NO_3)_2 \cdot 6\,H_2O$ dissolved in 5 mL ethanol was added to 1 g zeolite and then was dried at 80 °C for 18 h. The precursor salts were decomposed in air at 450 °C with a rate of 1 °C/min for 3h. The samples were denoted as **5Ni5Cu/Z** and **10Ni10Cu/Z**, respectively.

2.4. Characterization

X-ray powder diffraction patterns were recorded by Philips X'Pert type (Bruker AXS Advanced X-ray Solutions GmbH, Karlsruhe, Germany) diffractometer applying monochromatized Cu$K\alpha$ radiation (40 kV, 35 mA). Patterns were collected between 3 and 75 °2θ with 0.02° step size for 4 s. Crystallite size of the metal oxides were determined by the Sherrer equation evaluating the FWMH values of the oxide phases with full profile fitting method. The list of ICDD cards used for identification of metal oxide and metal phases are the following: CuO: 00-048-1548; NiO: 00-044-1159; Co_3O_4: 00-009-0418; $Co_{1.29}Ni_{1.71}O_4$: 00-040-1191; $Ni_{0.8}Cu_{0.2}O$: 00-078-0647; Ni^0: 00-045-1027; Cu^0: 00-004-0836; Co^0: 00-015-0806; $Cu_{0.81}Ni_{0.19}$: 00-047-1406; Ni_xCu_{1-x}: 01-066-0202.

Specific surface area and pore volume of the samples was determined from N_2 physisorption isotherms collected at −196 °C using AUTOSORB iQ-C-MP-AG-AG (Quantachrome Instruments, Anton Paar brand, Boynton Beach, FL, USA). Samples were pretreated at 350 °C in vacuum before nitrogen adsorption. Total pore volume was determined according to the Gurvich rule at relative pressure of 0.9.

The temperature-programmed reduction-thermogravimetric analysis (TPR-TGA) investigations were performed by a STA449F5 Jupiter type instrument of NETZSCH Gerätebau GmbH (Netzsch, Germany). In a typical measurement 20 mg of sample was placed in a microbalance crucible and heated in a flow of 5 vol. % H_2 in Ar (100 cm^3/min) up to 500 °C at a rate of 5 °C/min and a final hold-up of 1 h. Prior to the TPR experiments the samples were treated in situ in at 500 °C in air flow (10 °C/min) for 1 h.

The XPS measurements were carried out on AXIS Supra electron spectrometer (Kratos Analitycal Ltd. Manchester, UK) using AlK_α radiation with photon energy of 1486.6 eV. The energy calibration was performed by normalizing the C1s line of adsorbed adventitious hydrocarbons to 284.8 eV. The binding energies (BE) were determined with accuracy of ±0.1 eV using the commercial data-processing software ESCApe™ of Kratos Analytical Ltd. The concentrations of the different chemical elements (in atomic %) were calculated by normalizing the areas of the photoelectron peaks to their relative sensitivity factors. The deconvolution of the peaks has been performed by using the commercial data-processing software ESCApe™ of Kratos Analytical Ltd.

2.5. Catalytic experiments

Prior to the catalytic tests, samples were pretreated for 1 h in Ar/ H_2 flow at 500 °C, for 1 h, 1 °C/min. In a typical experiment, the reactor was charged with 1 g LA (Sigma-Aldrich, 98%), 20 mL H_2O and 0.2 g powder catalyst (mono and bimetallic, 200 mg catalyst/1 g LA) while the LA/H_2O weight ratio was maintained 1:10.

Levulinic acid hydrodeoxygenation was studied at atmospheric pressure using a reactor with hydrogen as carrier gas (30 mL/min). The reactor, heated under stirring with 700 rpm at the reaction

Preprints (www.preprints.org) | NOT PEER-REVIEWED | Posted: 1 December 2023 doi:10.20944/preprints202312.0001.v1

temperature of 150 °C for 4 h. The thermocouple was positioned in the reaction mixture for accurate measurement of the reaction temperature. Samples were taken every hour from the reaction mixture starting from 1 h reaction time and analyzed using HP-GC with a Shimadzu column, cat. Nº221-75940-30 Phase: SH-Rxi; -5MS; Size L30m.

3. Results and discussion

The XRD patterns (Figure 1) and the phase analysis of the initial zeolite support show the formation of the following crystalline phases: zeolite 13X (72 wt. %), zeolite A (LTA 3 wt. %), quartz (10 wt. %), dolomite (10 wt. %) and a spinel type iron-oxide, most probably maghemite (5 wt. %). The wide amorphous halo at about 25 °2θ is characteristic for non-crystallized alumino silica phase. Co_3O_4, CuO and NiO crystalline phases were registered on the relevant 10 wt.% metal containing, monocomponent catalysts. The crystallite size of the metal-oxide nanoparticles calculated by the Scherrer equation are presented in Table 1. Cobalt and nickel oxide show higher dispersion on zeolite support with 17-26 nm crystallite size, however CuO can be found in more agglomerated form with 35 nm sized nanoparticles. In nickel and copper containing bicomponent formulations both types of metal oxides appear with nickel in higher dispersion [46]. Formation of $Ni_{1-x}Cu_xO$ solid solution phase with x=0-0.2 approximate value is highly probable, because in NiO/CuO solid solution system incorporation of about 20% of copper was found to be the limit of a separate CuO phase appearance [47,48]. Replacement of Ni^{2+} ions by Cu^{2+} results in some increase in cubic, F*m*3*m* type unit cell parameter a_0 of NiO, due to the higher ionic radii of copper ion (Cu:0.73 Å, Ni: 0.69 Å). However, due to the small difference between the unit cells the differentiation with powder diffraction method is difficult, especially with widened reflections due to small crystallite size. Nevertheless, profile fitting with ICDD card No. 01-025-1049 ($Ni_{0.8}Cu_{0.2}O$) gives better result than NiO (01-044-1159). As could be expected higher metal content resulted in somewhat bigger crystallite size of the oxides, more enhanced for copper.

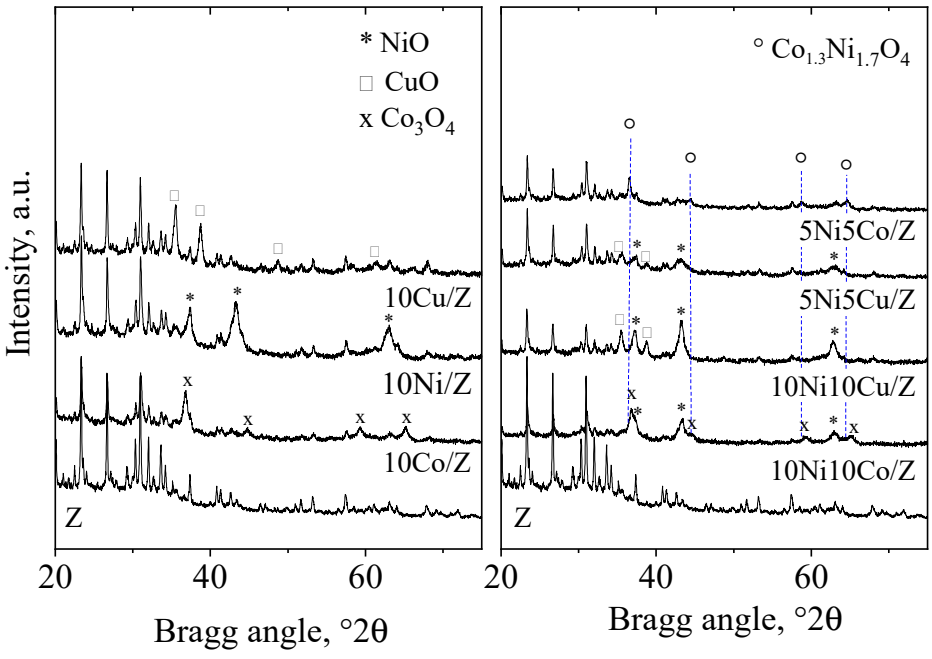

Figure 1. X-ray powder diffraction patterns of the parent, the mono- and bimetallic fly ash zeolites.

Table 1. Crystallite size of metal oxides, and reducibility of the studied catalysts.

Sample name	Crystalline phase	Crystallite size, (nm)	Reducibility, %
10 Ni/Z	NiO	17	100
10 Co/Z	Co_3O_4	26	79
10Cu/Z	CuO	35	100

Preprints (www.preprints.org) | NOT PEER-REVIEWED | Posted: 1 December 2023 doi:10.20944/preprints202312.0001.v1

10Ni10Co/Z	NiO	17	82
	$Co_{1.3}Ni_{1.7}O_4$	26	
	Co_3O_4	26	
10Ni10Cu/Z	NiO/ $Ni_{0.8}Cu_{0.2}O$	17	100
	CuO	35	
5Ni5Co/Z	$Co_{1.3}Ni_{1.7}O_4$	35	100
5Ni5Cu/Z	NiO/$Ni_{0.8}Cu_{0.2}O$	13	100
	CuO	21	

Separate NiO and Co_3O_4 crystalline phases were registered only in 10Ni10Co/Z sample, together with a nickel cobalt mixed oxide with composition of $Co_{1.3}Ni_{1.7}O_4$ (ICDD card No. 01-040-1191). NiO showed also higher dispersion than cobalt oxide. On 5Ni5Co/Z catalyst only the mixed oxide phase could be observed with somewhat lower dispersity.

N_2 adsorption/desorption isotherms of initial zeolite and its mono- and bimetallic modifications are presented in Figure 2. The isotherms of Z and its modified derivatives are a combination of type II and IV isotherms, typical for microporous zeolites with some mesopores [49]. Isotherms show H3 type of hysteresis loops, characteristic for slit like pores. The calculated textural parameters are summarized in Table 2. The modification of the initial fly ash zeolite with Co, Cu and/or Ni leads to significant decrease of the surface area and micropore volume, indicating the pore blocking of zeolite.

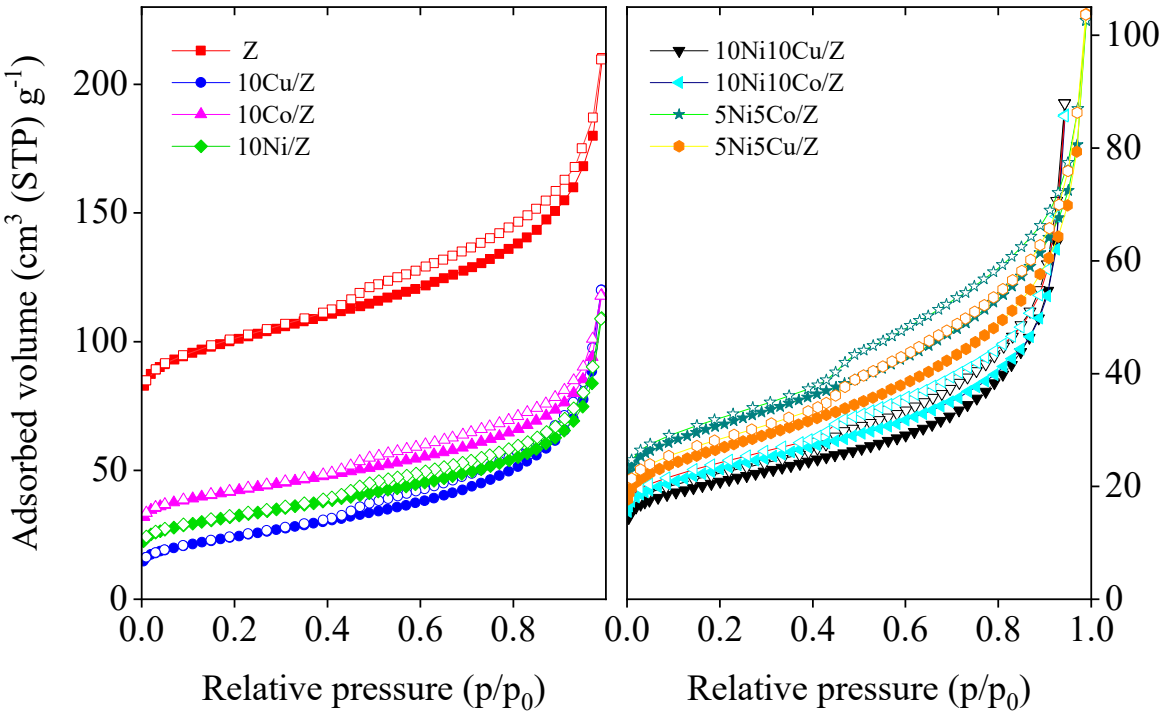

Figure 2. Nitrogen physisorption isotherms of the mono- and bimetallic fly ash zeolite materials.

Table 2. Textural properties of the studied catalysts.

Samples	S_{BET} (m^2/g)	Micropore volume (cm^3/g)	Total pore volume (cm^3/g)
10Ni/Z	115	0.019	0.169
10 Co/Z	152	0.034	0.183
10Cu/Z	86	0.006	0.186
10Ni10Co/Z	82	0.015	0.133
10Ni10Cu/Z	75	0.013	0.128
5Ni5Co/Z	111	0.020	0.159

Preprints (www.preprints.org) | NOT PEER-REVIEWED | Posted: 1 December 2023 doi:10.20944/preprints202312.0001.v1

5Ni5Cu/Z	96	0.015	0.160
Z	380	0.107	0.326
Samples reduced at 600 °C			
10Ni10Co/Z	181	0.047	0.130
5Ni5Co/Z	228	0.061	0.152
10Ni/Z	240	0.066	0.154

Most probably metal ions were incorporated into the zeolite lattice in cationic positions. Mesopore volume also decreased, showing that nanosized metal oxide deposits also occupied the pore system. To support the above ideas the nitrogen physisorption isotherms of some 600 °C reduced samples were also measured. Significant increase in specific surface area and micropore volume was experienced (Table 2), as evidence that upon reduction the metal ions and particles are migrated to the surface and made the pores accessible again to adsorbing gas. The zeolite structure remained also intact by reduction as proved by XRD results (not shown).

The redox properties of the mono- and bimetallic fly ash zeolite materials were studied by TPR experiments (Figure 3). The parent zeolite support contains 7 wt. % of iron. As typical for highly dispersed iron oxides the reduction takes place at about 400-450 °C, but iron can occupy also hardly reducible cationic positions. Accordingly, the TPR curve of fly ash zeolite shows peaks between 350 and 600 °C. The reduction rate is 100%, so most of the iron is reducible. The reduction of cobalt oxide on the fly ash zeolite is characterized by three steps at 325, 370 and 570 °C which points towards that a part of cobalt-oxide is finely dispersed on the support, but a similar part is hardly reducible. The latter one can be identified with cobalt ions in cationic position of zeolite or by formation of cobalt silicate.

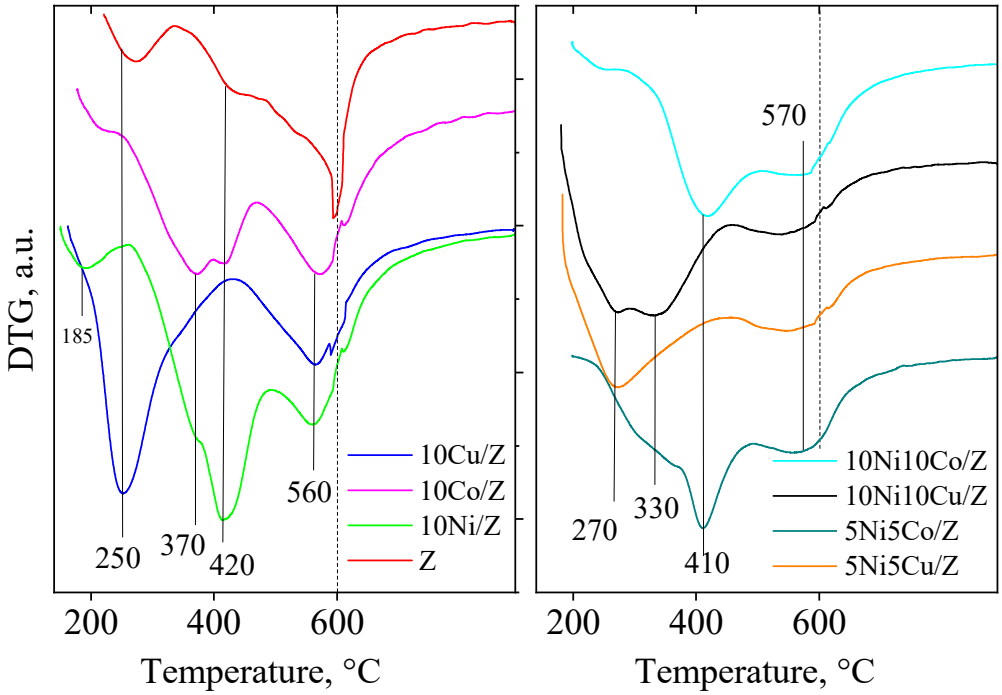

Figure 3. TPR-TG profiles of the studied catalysts.

Monometallic Ni-material can be reduced at similar temperature interval like cobalt sample, showing three reduction peaks at around 325, 420 and 570 °C, also indicating the formation of finely dispersed nickel oxide particles, and cationic nickel in the zeolite lattice.

In contrast, copper zeolite can be reduced in one intense step at much lower temperature, at 250 °C, and in a higher, but less intensive one over 560 °C. The identification is similar to the preceding ones, finely dispersed copper oxide on the external surface and copper ions in the zeolite lattice, respectively.

Preprints (www.preprints.org) | NOT PEER-REVIEWED | Posted: 1 December 2023 doi:10.20944/preprints202312.0001.v1

The modification with two metals resulted in significant changes in the reduction behavior of copper containing samples. The presence of copper enhanced the reducibility of nickel, most probably by the formation of an intermetallic phase with copper in majority [10].

Ni and cobalt containing catalysts can be reduced in the same temperature range as the individual components, i.e., over 400 °C. The extent of metal oxide reduction is calculated based on the amount of hydrogen consumption during reduction and the results are presented in Table 1. Total reduction was calculated for all the samples except 10Ni10Co/Z catalyst. This can be in connection with the formation of hardly reducible cobalt silicate in connection with the high concentration of metals in the catalyst.

The surface composition of bimetallic samples with 20% metal content were analyzed by X-ray photoelectron spectroscopic (XPS) method. The spectra of 10Ni10Co/Z, 10Ni10Cu/Z are presented in Figure 4. The calculated compositions are summarized in Table 3. The Ni $2p_{3/2}$ peak with binding energy of 853.7 eV is characteristic for Ni^{2+} in NiO [50] and its shift to higher binding energy (854.3 eV) for both samples is indicative for the possible interaction with Si or Cu/Co. The peaks in the Cu $2p_{3/2}$ spectrum at 933.4 eV and the presence of the characteristic satellites support the XRD data, indicating the presence of CuO phase [51]. In the $Co2p_{3/2}$ spectrum, the peaks at 779.2 (Co^{3+}) and 780.8 (Co^{2+}) eV support the formation of spinel Co_3O_4 (Figure 4). The surface chemical composition mirrors the crystalline phases of the catalysts with the presence of Fe, Ca, and Mg, whereas Na, Si, and Al as the main constituents of zeolite and amorphous silica alumina phase. The amount of catalytically active Ni, Cu and Co elements differs from that of bulk value, the nickel is overrepresented 2-3 times on the surface. This can be explained by the formation of nickel rich mixed oxides and the interaction of copper and cobalt with the silica matrix. The presence of bigger copper and cobalt oxide nanoparticles can be another reason, in accordance with XRD results.

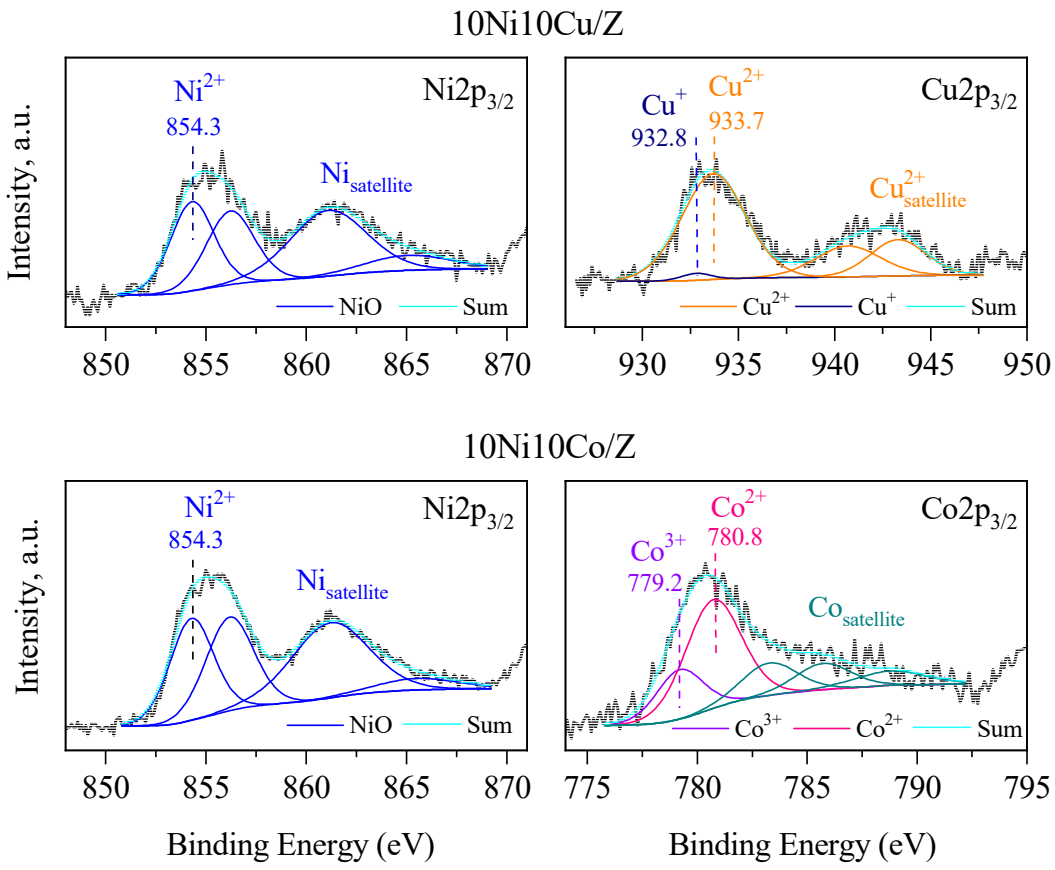

Figure 4. XPS spectra of the 10Ni10Co/Z and 10Ni10Cu/Z catalysts.

Table 3. XPS data of 10Ni10Co/Z and 10Ni10Cu/Z catalysts.

Composition, at. %	Cu	Ni	Co	Si	Al	O	Fe	Na	Ca	Mg

Preprints (www.preprints.org) | NOT PEER-REVIEWED | Posted: 1 December 2023 doi:10.20944/preprints202312.0001.v1

10Ni10Cu/Z	3.2	7.3	-	10.4	4.5	61.4	3.9	6.5	1.4	1.4
10Ni10Co/Z	-	11.4	3.9	9.1	3.5	60.3	5.0	4.0	1.3	1.5

The catalytic activity of the mono-metallic and bimetallic zeolites was studied in hydrodeoxygenation of levulinic acid to γ-valerolactone at 150 °C reaction temperature, and the results are presented in Table 4.

Table 4. Catalytic data for the hydrodeoxygenation of levulinic acid on the studied catalysts.

Catalysts	Conversion, %	HPA yield, %	GVL yield, %
10Ni/Z	35.0	8.0	27.0
10Co/Z	2.7	0.8	1.9
10Cu/Z	5.9	1.1	4.8
5Ni5Co/Z	51.0	7.0	44.0
5Ni5Cu/Z	63.0	10.0	53.0
10Ni10Co/Z	99.5	14.8	84.7
10Ni10Cu/Z	100.0	15.0	85.0

The main detected products in the reaction are γ-valerolactone (GVL) and 4-hydroxy pentanoic acid (HPA). Low catalytic activity was registered for cobalt and copper containing monometallic catalysts. However, 10Ni/Z showed almost 10 times higher activity than the former ones. Significant increase in the catalytic activity was observed for the bimetallic catalysts, especially with increased metal content, with about 100% conversion. The γ-valerolactone yield exceeded than that of 4-hydroxy pentanoic acid in each case. According to Scheme 1, the formation of GVL is reported via two possible pathways. When dehydrogenation reaction step is more decisive, Path I proceeds by the formation of α-angelica lactone, and it is rather characteristic for the hydrodeoxygenation reaction in the vapor phase [10]. In liquid phase reaction, 4-hydroxypentanoic acid is experienced to be the typical intermediate in the consecutive reaction, due to lower reaction temperature, thermodynamically favoring the hydrogenation as a first reaction step. Based on the obtained reaction products we suppose that Path II is dominating the reaction (Scheme 1) without a further hydrogenation step to pentanoic acid. The synergistic effect of bimetallic catalysts is well-marked compared to monometallic ones. One explanation can be the formation of mixed oxide phases in connection with improved reducibility of the active components. However, the amount of metals plays also crucial role. With higher metal content the formation active metallic phase by reduction is more pronounced, due to lower interaction with support, and formation of highly dispersed metallic phases.

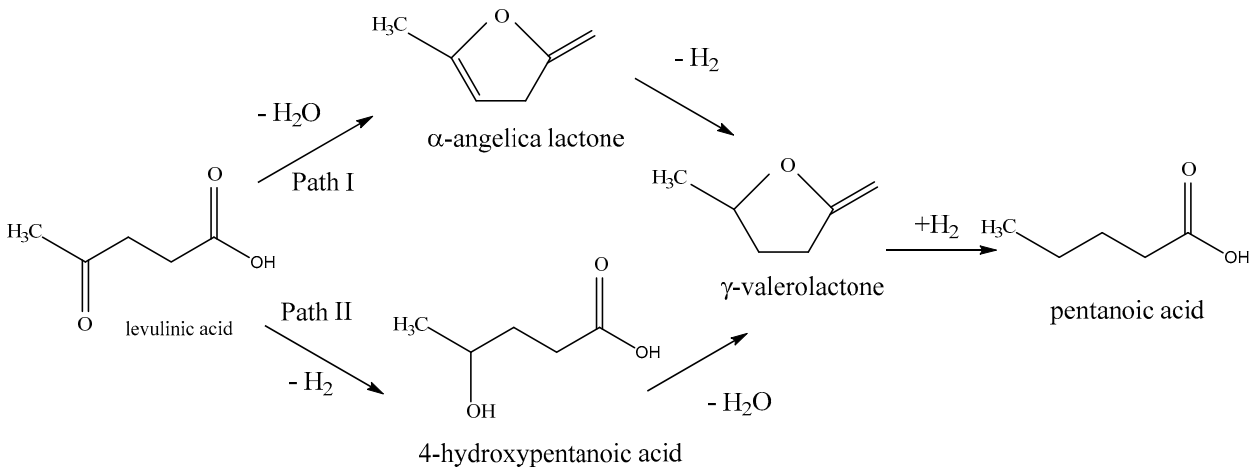

Scheme 1. Reaction mechanisms of LA hydrodeoxygenation to GVL.

Preprints (www.preprints.org) | NOT PEER-REVIEWED | Posted: 1 December 2023 doi:10.20944/preprints202312.0001.v1

Investigation of spent catalysts revealed some other important characteristics of catalytic system. The XRD patterns of the four most active catalysts are shown in Figure 5. The absence of crystalline zeolite phase is evident, and formation of only metallic phases is experienced. Nitrogen physisorption data (Table 5) support the lack of zeolite phase, because micropores cannot be detected in the samples. However, the surface area of the amorphous silica alumina is high enough to serve as a catalyst support, and the increased pore volume values indicate the reconstruction of the pore system. The phenomena of amorphization can be explained by using water as a solvent, promoting hydrothermal decomposition of the zeolite. Investigating the phase composition of metallic nanoparticles formed by reduction, formation of intermetallic phases is highly probable, especially in Ni/Co composition, because of the similarities of the ion size and cubic unit cell of the two metals, however by XRD method the substitution of ions cannot be proved. Formation of NiCu alloys was identified on both Ni/Cu catalysts, but with different compositions. In 5Ni5Cu/Z sample the ratio of the metals was equal, based on the calculation of unit cell size of the cubic system (a_0=3.56 Å), according to Vegard's law, presented by the works of Smirnov et. al. [52,53]. In 10Ni10Cu/Z sample the presence of copper rich phases was detected. The dispersion of metals was higher than that of metal oxides in the parent catalysts.

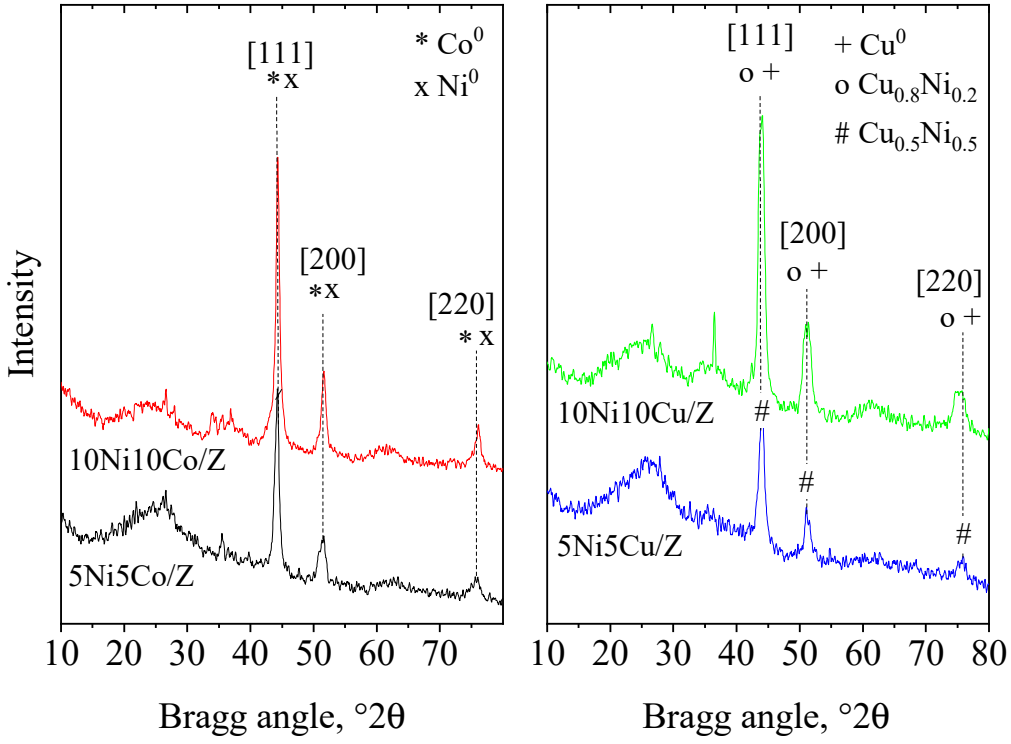

Figure 5. XRD patterns of spent bimetallic catalysts.

Table 5. Textural parameters of spent catalysts and the crystallite size of reduced metals.

Samples	S_{BET} (m^2/g)	Total pore volume (cm^3/g)	Crystalline phases	Crystallite size, nm
10Ni10Co/Z spent	275	0.462	Ni^0/Co^0	21
10Ni10Cu/Z spent	271	0.422	Cu^0, $Cu_{0.81}Ni_{0.19}$	13/13
5Ni5Co/Z spent	256	0.379	Ni^0/Co^0	19
5Ni5Cu/Z spent	279	0.400	Ni_xCu_{1-x} (x~0.5)	13

4. Conclusions

Monometallic (Ni, Cu, Co) and bimetallic (Ni-Co, Ni-Cu) catalysts supported on fly ash zeolite were prepared by post synthesis impregnation method. Formation of metal oxides and mixed metal

oxides was detected on the support. Blocking of micropore and mesopore system by metal ions and highly dispersed metal oxides was also an accompanying phenomenon. By reducing the catalysts, the pore system became permeable again. TPR experiments proved the favorable effect of bimetallic systems on improved reducibility with Ni/Cu compositions. XPS study revealed the enrichment of nickel on the surface on bimetallic compositions with high metal content. In accordance with physico-chemical characterization results, high catalytic activity was detected for levulinic acid hydrodeoxygenation to γ-valerolactone on bimetallic catalysts with 20 wt. % metal content. Besides the total conversion, the yield to GVL was also high, over 80%. Investigation of spent catalysts showed the collapse of zeolite structure and reorganization of pore system, creating a high surface area amorphous silica-alumina supported Ni/Co, Ni/Cu catalytic system.

Funding: This work was supported by Bulgarian National Science Fund, Grant КП-06-Н69/3 is acknowledged. Support of this work in the framework of the bilateral grant agreement between the Bulgarian Academy of Sciences and the Hungarian Academy of Sciences (IC-HU/02/2022-2023) is also gratefully acknowledged.

References

1. Climent, M.J.; Corma, A.; and Iborra, S. Conversion of biomass platform molecules into fuel additives and liquid hydrocarbon fuels. *Green Chem.* **2014**, *16, 516–547*. doi: 10.1039/c3gc41492b.
2. Mika, L.T.; Cséfalvay, E.; and Németh Á. Catalytic conversion of carbohydrates to initial platform chemicals: chemistry and sustainability. *Chem. Rev.* **2018**, *118, 505–613*. doi: 10.1021/acs.chemrev.7b00395.
3. Li, H.; Fang, Zh.; Smith, R.L.Jr.; and Yang, S. Efficient valorization of biomass to biofuels with bifunctional solid catalytic materials. *Prog. Energy Combust.* Sci. **2016**, *55, 98–194*. doi: 10.1016/j.pecs.2016.04.004.
4. Catalán-Martínez, D.; Domine, M.E.; and Serra J.M. Liquid fuels from biomass: An energy self-sustained process integrating H_2 recovery and liquid refining. *Fuel* **2018**, *212, 353-363*. doi: 10.1016/j.fuel.2017.10.014.
5. Alper, K.; Tekin, K.; Karagöz, S.; and Ragauskas, A.J. Sustainable energy and fuels from biomass: a review focusing on hydrothermal biomass processing. ***Sustain. Energy Fuels*** **2020**, ***4***, *4390-4414*. doi: 10.1039/D0SE00784F.
6. Xuan, J.; Leung, M.K.H.; Leung D.Y.C.; and Ni M. A review of biomass-derived fuel processors for fuel cell systems. *Renew. Sustain. Energy Rev.* **2009**, *13, 1301-1313*. doi: 10.1016/j.rser.2008.09.027.
7. Serrano-Ruiz, J.C.; Luque R.; and Sepúlveda-Escribano A. Transformations of biomass-derived platform molecules: from high added-value chemicals to fuels *via* aqueous-phase processing. ***Chem. Soc. Rev.*** **2011**, ***40***, *5266-5281*. doi: 10.1039/C1CS15131B.
8. Devi, A.; Bajar, S.; Kour, H.; Kothari, R.; Pant, D.; and Singh, A. Lignocellulosic biomass valorization for bioethanol production: a circular bioeconomy approach. *BioEnergy Res.* **2022**, *15, 1820–1841*. doi: 10.1007/s12155-022-10401-9.
9. Horváth, I.T.; Mehdi, H.; Fábos, V.; Boda, L.; and Mika, L.T. γ-Valerolactone–a sustainable liquid for energy and carbon-based chemicals. *Green Chem.* **2008**, *10, 238–242*. doi: 10.1039/B712863K.
10. Dutta, Sh.; Yu, I.K.M.; Tsang, D.C.W.; Ng, Y.H.; Ok, Y.S.; Sherwood, J.; and Clark, J.H. Green synthesis of gamma-valerolactone (GVL) through hydrogenation of biomass-derived levulinic acid using non-noble metal catalysts: A critical review. *Chem. Eng. J.* **2019**, *372, 992-1006*. doi:10.1016/j.cej.2019.04.199.
11. Galletti, A.M.R.; Antonetti, C.; De Luise, V.; and Martinelli, M. A sustainable process for the production of γ-valerolactone by hydrogenation of biomass-derived levulinic acid. *Green Chem.* **2012**, *14, 688–694*. doi: 10.1039/c2gc15872h.
12. Long, X.; Sun, P.; Li, Z.; Lang, R.; Xia, Ch.; and Li, F. Magnetic Co/Al_2O_3 catalyst derived from hydrotalcite for hydrogenation of levulinic acid to γ-valerolactone. *Chin. J. Catal.* **2015**, *36, 1512–1518*. doi: 10.1016/S1872-2067(15)60934-2.
13. Adeleye, A.T.; Louis, H.; Akakuru, O.U.; Joseph, I., Enudi, O.C.; and Michae, D.P. A review on the conversion of levulinic acid and its esters to various useful chemicals, *AIMS Energy* **2019**, *7, 165–185*. doi: 10.3934/energy.2019.2.165.
14. Sosa, L.F.; da Silva, V.T.; and de Souza, P.M. Hydrogenation of levulinic acid to γ-valerolactone using carbon nanotubes supported nickel catalysts. *Cat. Tod.* **2021**, *381, 86-95*. doi: 10.1016/j.cattod.2020.08.022.
15. Yanase, D.; Hara, T., Sato, F.; Yamada, Y.; and Sato, S. Vapor-phase hydrogenation of levulinic acid to γ-valerolactone over Cu-Ni alloy catalysts. *Appl. Cat. A* **2021**, *616, 118093*. doi: 10.1016/j.apcata.2021.118093.

16. Yu, Z.; Lu, X.; Xiong, J.; Li, X.; Bai, H.; and Ji, N. Heterogeneous catalytic hydrogenation of levulinic acid to γ-valerolactone with formic acid as internal hydrogen source. *Chem. Sus. Chem.* **2020**, *13, 2916-2930*. doi: 10.1002/cssc.202000175.
17. Liu, Q.; Zhou, H.; and Jia, Z. Hydrogen production by ethanol reforming on Supported Ni–Cu catalysts, ACS Omega **2022**, *7, 4577–4584*. doi: 10.1021/acsomega.1c06579.
18. Li, T.; Su, H.; Zhu, L.; Xu D.; Ji N.; and Wang, S. Hydrogen production from steam reforming of biomass-derived levulinic acid over highly stable spinel-supported Ni catalysts. *Waste Dispos. Sustain. Energy* **2023**. doi: 10.1007/s42768-023-00154-2.
19. Robertson, S.D.; McNicol, B.D.; De Baas, J.H.; Kloet, S.C.; and Jenkins J.W. Determination of reducibility and identification of alloying in copper-nickel-on-silica catalysts by temperature-programmed reduction, *J. Cat.* **1975**, *37, 424-431*. doi: 10.1016/0021-9517(75)90179-7.
20. López-Fonseca, R.; Jiménez-González, C.; de Rivas, B.; and Gutiérrez-Ortiz, J. I. Partial oxidation of methane to syngas on bulk $NiAl_2O_4$ catalyst. Comparison with alumina supported nickel, platinum, and rhodium catalysts. *Appl. Catal. A* **2012**, *437, 53–62*. doi: 10.1016/j.apcata.2012.06.014.
21. Popova, M.; Djinović, P.; Ristić, A.; Lazarova, H.; Dražić, G.; Pintar, A.; Balu, A.M.; and Tušar N.N. Vapor-phase hydrogenation of levulinic acid to γ-valerolactone over bi-functional Ni/HZSM-5 catalyst, *Front. Chem.* **2018**, *6, 285*. doi: 10.3389/fchem.2018.00285.
22. Upare, P.P.; Lee, J.-M.; Hwang, D.W.; Halligudi, S.B.; Hwang, Y.K.; and Chang, J.-S. Selective hydrogenation of levulinic acid to γ-valerolactone over carbon-supported noble metal catalysts. *J. Indust. Eng. Chem.* **2011**, *17, 287-292*. doi: 10.1016/j.jiec.2011.02.025.
23. Xue, Z.; Liu, Q.; Wang, J.; and Mu, T. Valorization of levulinic acid over non-noble metal catalysts: challenges and opportunities. ***Green Chem.*** **2018**, *20, 4391-4408*. doi: 10.1039/C8GC02001A.
24. Hengne, A.M.; Kadu, B.S.; Biradar, N.S.; Chikate, R.C.; and Rode, C.V. Transfer hydrogenation of biomass-derived levulinic acid to γ-valerolactone over supported Ni catalysts. ***RSC Adv.*** **2016**, ***6***, *59753-59761*. doi: 10.1039/C6RA08637C.
25. Song, S.; Yao, S.; Cao, J.; Di, L.; Wu, G.; Guan, N.; and Li, L. Heterostructured Ni/NiO composite as a robust catalyst for the hydrogenation of levulinic acid to –valerolactone, **2017**, *217, 115-124*. doi: 10.1016/j.apcatb.2017.05.073.
26. Huang, X.; Liu, K.; Vrijburg, W.L.; Ouyang, X.; Dugulan, A.I.; Liu, Y. Verhoeven M.W.G.M.T., Kosinov, N.A., Pidko, E.A., and Hensen, E.J.M. Hydrogenation of levulinic acid to γ-valerolactone over Fe-Re/TiO_2 catalysts. *Appl. Cat. B: Environmental* **2020**, *278, 119314*. doi: 10.1016/j.apcatb.2020.119314.
27. Gebresillase, M.N.; Raguindin, R.Q.; Kim, H.; and Seo, J.G. Supported bimetallic catalysts for the solvent-free hydrogenation of levulinic acid to γ-valerolactone: effect of metal combination (Ni-Cu, Ni-Co, Cu-Co). *Catalysts* **2020**, *10, 1354*. doi: 10.3390/catal1011135.
28. Yanase, D.; Yoshida, R.; Kanazawa, S.; Yamada, Y.; and Sato, S. Efficient formation of γ-valerolactone in the vapor-phase hydrogenation of levulinic acid over Cu-Co/alumina catalyst. *Cat. Commun*. **2020**, *139, 105967*. doi: 10.1016/j.catcom.2020.105967.
29. Wang, J.; Liu, J.; Yu, X.; Zhang, W.; Zhang, G.; Liu, M.; Shen, J.; Yang, C.; and Jin, X. Non-noble metal catalysts for transfer hydrogenation of levulinic acid: The role of surface morphology and acid-base pairs, *Mat. Tod. Energy* **2020**, *18, 100501*. doi: 10.1016/j.mtener.2020.100501.
30. Derle, S.N.; and Parikh, P.A. Hydrogenation of levulinic acid and γ-valerolactone: steps towards biofuels. *Biomass Conv. Bioref.* **2014**, *4, 293–299*. doi: 10.1007/s13399-013-0111-5.
31. Hattori, H.; and Ono, Y. Catalysts and catalysis for acid-base reactions, In: Metal oxides in heterogeneous catalysts, Eds, J.C. Vedrine, Elsevier Inc., 2018, pp. 133-209, doi: 10.1016/C2016-0-01790-4.
32. Boycheva, S.; Szegedi, Á.; Lázár, K.; Popov, C.; and Popova, M. Advanced high-iron coal fly ash zeolites for low-carbon emission catalytic combustion of VOCs. *Cat. Today* **2023**, *418, 114109*, doi: 10.1016/j.cattod.2023.114109.
33. Michalev, T.; and Petrov, I. The removal of heavy metal ions by synthetic zeolites: A review, *Proceedings of the University of Ruse* **2012**, *51, 79-84*. ISSN 2603-4123.
34. Feng, W.; Lu, X.; Xiong, J.; Yu, Z.; Wang, Y.; Cui, J.; Zhang, R.; and Weng, R. Solid–waste–derived geopolymer–type zeolite–like high functional catalytic materials catalyze efficient hydrogenation of levulinic acid. *Catalysts* **2022**, *12*, 1361. doi: 10.3390/catal12111361.

35. Tian, Y.; Zhu, X.; Zhou, S.; Zhao, W.; Xu, Q.; and Liu, X. Efficient synthesis of alkyl levulinates fuel additives using sulfonic acid functionalized polystyrene coated coal fly ash catalyst. *J. Biores. Bioprod.* **2023**, *8, 198-213*. doi: 10.1016/j.jobab.2023.01.003.
36. Gong, L.; Xu, Z.-Y.; Dong, J.-J.; Li, H.; Han, R.-Z.; Xu, G.-C.; and Ni, Y. Composite coal fly ash solid acid catalyst in synergy with chloride for biphasic preparation of furfural from corn stover hydrolysate. *Biores. Technol.* **2019**, *293, 122065*. doi: 10.1016/j.biortech.2019.122065.
37. Alterary, S.S.; and Marei, N.H. Fly ash properties, characterization, and applications: A review. *J. King Saud Uni. – Sci.* **2021**, *33, 101*536. doi: 10.1016/j.jksus.2021.101536.
38. Popova, M.; Boycheva, S.; Lazarova, H.; Zgureva, D.; Lázár, K.; and Szegedi, Á. VOC oxidation and CO_2 adsorption on dual adsorption/catalytic system based on fly ash zeolites, *Cat.Today* **2020**, *357, 518-525*. doi: 10.1016/j.cattod.2019.06.070.
39. Boycheva, S.; Zgureva, D.; Václavíková, M.; Kalvachev, Y.; Lazarova, H.; and Popova, M. Studies on non-modified and copper-modified coal ash zeolites as heterogeneous catalysts for VOCs oxidation. *J. Haz. Mat.* **2019**, *361, 374-382*. doi: 10.1016/j.jhazmat.2018.07.020.
40. Boycheva, S.; Marinov, I.; Miteva, S.; and Zgureva, D. Conversion of coal fly ash into nanozeolite Na-X by applying ultrasound assisted hydrothermal and fusion-hydrothermal alkaline activation. Sustain. *Chem. Pharm.* **2020**, *15, 100217*. doi: 10.1016/j.scp.2020.100217.
41. Boycheva, S.; Zgureva, D.; Lazarova, K.; Babeva, T.; Popov, C.; Lazarova, H.; and Popova, M. Progress in the utilization of coal fly ash by conversion to zeolites with green energy applications. *Materials* **2020**, *13, 2014*. doi: 10.3390/MA13092014.
42. Belviso, C.; Cavalcante, F.; Di Gennaro, S.; Palma, A.; Ragone, P.; and Fiore, S. Mobility of trace elements in fly ash and in zeolitised coal fly ash. *Fuel* **2015**, *144, 369-379*. doi: 10.1016/j.fuel.2014.12.037.
43. Boycheva, S.; Zgureva-Filipova, D.; Popov, C.; Lazarova, H.; and Popova, M. Plasma-modified coal fly ash zeolites with enhanced catalytic efficiency toward the total oxidation of volatile organic compounds as low-cost substitutes for platinum group metals catalysts. *Phys. Stat. Sol. (A)* **2022**, *219, art. no. 2100632*. doi: 10.1002/pssa.202100632.
44. Boycheva, S.; Zgureva, D.; Lazarova, H.; and Popova, M. Comparative studies of carbon capture onto coal fly ash zeolites Na-X and Na–Ca-X. *Chemosphere* **2021**, *271, art. no. 129505*. doi: 10.1016/j.chemosphere.2020.129505.
45. Boycheva, S.; Miteva, S.; Zgureva, D.; and Marinov, I. Characterization of fly ashes from thermal power plants in Bulgaria supplied by lignite coal, In proceedings of XXVIII Scientific symposium with international participation "Situation in Ecologically loaded regions of Slovakia and Central Europe, 2019, 24–25 October 2019, Slovakia, Hrádok, pp. 97-104, ISBN 978-80-89883-10-3.
46. Tangcharoen, T.; Klysubun, W.; Kongmark, Composition Dependence of Structural, Optical, Magnetic and Photodegradation Properties of Nanocrystalline NiO/CuO Heterostructured Powders, *Ch. Phys. Status Solidi A* **2022**, *219, 2200072. DOI:10.1002/pssa.202200072*
47. Bularzik, J.; Davies, P. K.; Navrotsky, A. Thermodynamics of Solid-Solution Formation in NiO-CuO, *J. Am. Ceram. Soc.* **1986**, *69, 453-57*. https://doi.org/10.1111/j.1151-2916.1986.tb07444.x.
48. Fedorov, A. V.; Kukushki, R. G.; Yeletsky, P. M.; Bulavchenko, O. A.; Chesalov, Y. A.; Yakovlev, V. A. Temperature-programmed reduction of model CuO, NiO and mixed CuO–NiO catalysts with hydrogen\, *Journal of Alloys and Compounds* **2020**, *844, 156*135. https://doi.org/10.1016/j.jallcom.2020.156135.
49. Thommes, M.; Kaneko, K.; Neimark, A.V.; Olivier, J.P.; Rodriguez-Reinoso, F.; Rouquerol, J.; and Sing, K.S.W. Physisorption of gases, with special reference to the evaluation of surface area and pore size distribution (IUPAC Technical Report). *Pure Appl. Chem.* **2015,** https://doi.org/10.1515/pac-2014-1117
50. Biesinger, M. C.; Payne, B. P.; Grosvenor, A. P.; Lau, L. W.M.; Gerson, A. R.; Smart, R. St. C. Resolving surface chemical states in XPS analysis of first row transition metals, oxides and hydroxides: Cr, Mn, Fe, Co and Ni, Applied Surface Science 257 (2011) 2717–2730, https://doi.org/10.1016/j.apsusc.2010.10.051.
51. Biesinger, M. C. Advanced analysis of copper X-ray photoelectron spectra, *Surf. Interface Anal.* **2017**, *49, 1325–1334*, https://doi.org/10.1002/sia.6239.
52. Smirnov, A. A. Khromova, S. A. Bulavchenko, O. A. Kaichev, V. V. Saraev, A. A. Reshetnikov, S. I. Bykova, M. V. Trusov, L. I. and Yakovlev, V. A. Effect of the Ni/Cu ratio on the composition and catalytic properties of nickel-copper alloy in anisole hydrodeoxygenation, *Kinetics and Catalysis* **2014**, *55, 69–78*. https://doi.org/10.1134/S0023158414010145

53. Smirnov, A.A.; Khromova, S.A.; Bulavchenko, O.A.; Kaichev, V.V.; Saraev, A.A.; Reshetnikov, S.I.; Bykova, M.V.; Trusov, L.I.; Yakovlev V.A. Effect of the Ni/Cu Ratio on the Composition and Catalytic Properties of Nickel–Copper Alloy in Anisole Hydrodeoxygenation, *Kinetika i Kataliz*, **2014**, *55*, *72–81*. doi: 10.1134/S0023158414010145.